Ultrabroadband terahertz conductivity of highly doped ZnO and ITO

Wang, Tianwu; Zalkovskij, Maksim; Iwaszczuk, Krzysztof; Lavrinenko, Andrei; Naik, Gururaj V.; Kim, Jongbum; Boltasseva, Alexandra; Jepsen, Peter Uhd

Published in:
Optical Materials Express

Link to article, DOI:
10.1364/OME.5.000566

Publication date:
2015

Document Version
Publisher's PDF, also known as Version of record

Ultrabroadband terahertz conductivity of highly doped ZnO and ITO

Tianwu Wang,[1,3,*] Maksim Zalkovskij,[1,3] Krzysztof Iwaszczuk,[1] Andrei V. Lavrinenko,[1] Gururaj V. Naik,[2] Jongbum Kim,[2] Alexandra Boltasseva,[1,2] and Peter Uhd Jepsen[1]

[1]*DTU Fotonik - Department of Photonics Engineering, Technical University of Denmark, DK-2800 Kongens Lyngby, Denmark*

[2]*Birck Nanotechnology Center and School of Electrical & Computer Engineering, Purdue University, West Lafayette, Indiana 47906, USA*

[3]*The authors contributed equally to this work*

[*]*tianw@fotonik.dtu.dk*

Abstract: The broadband complex conductivities of transparent conducting oxides (TCO), namely aluminum-doped zinc oxide (AZO), gallium-doped zinc oxide (GZO) and tin-doped indium oxide (ITO), were investigated by terahertz time domain spectroscopy (THz-TDS) in the frequency range from 0.5 to 18 THz using air plasma techniques, supplemented by the photoconductive antenna (PCA) method. The complex conductivities were accurately calculated using a thin film extraction algorithm and analyzed in terms of the Drude conductivity model. All the measured TCOs have a scattering time below 15 fs. We find that a phonon response must be included in the description of the broadband properties of AZO and GZO for an accurate extraction of the scattering time in these materials, which is strongly influenced by the zinc oxide phonon resonance tail even in the low frequency part of the spectrum. The conductivity of AZO is found to be more thickness dependent than GZO and ITO, indicating high importance of the surface states for electron dynamics in AZO. Finally, we measure the transmittance of the TCO films from 10 to 200 THz with Fourier transform infrared spectroscopy (FTIR) measurements, thus closing the gap between THz-TDS measurements (0.5-18 THz) and ellipsometry measurements (200-1000 THz).

OCIS codes: (310.0310) Thin films; (310.6860) Thin films, optical properties; (300.6495) Spectroscopy, terahertz.

References and links

1. J. B. Khurgin and A. Boltasseva, "Reflecting upon the losses in plasmonics and metamaterials," MRS Bull. **37**(08), 768–779 (2012).
2. A. Boltasseva and H. A. Atwater, "Materials science. Low-loss plasmonic metamaterials," Science **331**(6015), 290–291 (2011).
3. G. V. Naik, V. M. Shalaev, and A. Boltasseva, "Alternative plasmonic materials: beyond gold and silver," Adv. Mater. **25**(24), 3264–3294 (2013).
4. J. S. Kim, J.-H. Jeong, J. K. Park, Y. J. Baik, I. H. Kim, T.-Y. Seong, and W. M. Kim, "Optical analysis of doped ZnO thin films using nonparabolic conduction-band parameters," J. Appl. Phys. **111**(12), 123507 (2012).
5. G. V. Naik, J. Kim, and A. Boltasseva, "Oxides and nitrides as alternative plasmonic materials in the optical range," Opt. Mater. Express **1**(6), 1090–1099 (2011).
6. G. V. Naik, J. Liu, A. V. Kildishev, V. M. Shalaev, and A. Boltasseva, "Demonstration of Al:ZnO as a plasmonic component for near-infrared metamaterials," Proc. Natl. Acad. Sci. U.S.A. **109**(23), 8834–8838 (2012).
7. J. Kim, G. V. Naik, A. V. Gavrilenko, K. Dondapati, V. I. Gavrilenko, S. M. Prokes, O. J. Glembocki, V. M. Shalaev, and A. Boltasseva, "Optical properties of gallium-doped zinc oxide—A low-loss plasmonic material: first-principles theory and experiment," Phys. Rev. X **3**, 041037 (2013).

#228530 - $15.00 USD Received 25 Nov 2014; revised 29 Jan 2015; accepted 3 Feb 2015; published 12 Feb 2015

8. C.-W. Chen, Y.-C. Lin, C.-H. Chang, P. Yu, J.-M. Shieh, and C.-L. Pan, "Frequency-dependent complex conductivities and dielectric responses of indium tin oxide thin films from the visible to the far-Infrared," IEEE J. Quantum Electron. **46**(12), 1746–1754 (2010).
9. M. Walther, D. G. Cooke, C. Sherstan, M. Hajar, M. R. Freeman, and F. A. Hegmann, "Terahertz conductivity of thin gold films at the metal-insulator percolation transition," Phys. Rev. B **76**(12), 125408 (2007).
10. T.-I. Jeon and D. Grischkowsky, "Nature of conduction in doped silicon," Phys. Rev. Lett. **78**(6), 1106–1109 (1997).
11. T.-I. Jeon and D. Grischkowsky, "Observation of a Cole–Davidson type complex conductivity in the limit of very low carrier densities in doped silicon," Appl. Phys. Lett. **72**(18), 2259 (1998).
12. X. Xie, J. Dai, and X.-C. Zhang, "Coherent control of THz wave generation in ambient air," Phys. Rev. Lett. **96**(7), 075005 (2006).
13. J. Dai, X. Xie, and X.-C. Zhang, "Detection of broadband terahertz waves with a laser-induced plasma in gases," Phys. Rev. Lett. **97**(10), 103903 (2006).
14. D. Zhang, Z. Lü, C. Meng, X. Du, Z. Zhou, Z. Zhao, and J. Yuan, "Synchronizing terahertz wave generation with attosecond bursts," Phys. Rev. Lett. **109**(24), 243002 (2012).
15. M. Zalkovskij, C. Z. Bisgaard, A. Novitsky, R. Malureanu, D. Savastru, A. Popescu, P. U. Jepsen, and A. V. Lavrinenko, "Ultrabroadband terahertz spectroscopy of chalcogenide glasses," Appl. Phys. Lett. **100**(3), 031901 (2012).
16. T. Wang, P. Klarskov, and P. U. Jepsen, "Ultrabroadband THz time-domain spectroscopy of a free-flowing water film," IEEE Trans. Terahertz Sci. Technol. **2014**, 1–7 (2014).
17. P. U. Jepsen, D. G. Cooke, and M. Koch, "Terahertz spectroscopy and imaging - Modern techniques and applications," Laser Photonics Rev. **5**(1), 124–166 (2011).
18. P. Klarskov, A. C. Strikwerda, K. Iwaszczuk, and P. U. Jepsen, "Experimental three-dimensional beam profiling and modeling of a terahertz beam generated from a two-color air plasma," New J. Phys. **15**(7), 075012 (2013).
19. A. Gorodetsky, A. D. Koulouklidis, M. Massaouti, and S. Tzortzakis, "Physics of the conical broadband terahertz emission from two-color laser-induced plasma filaments," Phys. Rev. A **89**(3), 033838 (2014).
20. N. Karpowicz, J. Dai, X. Lu, Y. Chen, M. Yamaguchi, H. Zhao, X.-C. Zhang, L. Zhang, C. Zhang, M. Price-Gallagher, C. Fletcher, O. Mamer, A. Lesimple, and K. Johnson, "Coherent heterodyne time-domain spectrometry covering the entire "terahertz gap,"," Appl. Phys. Lett. **92**(1), 011131 (2008).
21. S. Wei and M. Y. Chou, "Phonon dispersions of silicon and germanium from first-principles calculations," Phys. Rev. B Condens. Matter **50**(4), 2221–2226 (1994).
22. C. S. Wang, J. M. Chen, R. Becker, and A. Zdetsis, "Second order raman spectrum and phonon density of states of silicon," Phys. Lett. **44A**(7), 517–518 (1973).
23. X. Li, Z. Hong, J. He, and Y. Chen, "Precisely optical material parameter determination by time domain waveform rebuilding with THz time-domain spectroscopy," Opt. Commun. **283**(23), 4701–4706 (2010).
24. I. Pupeza, R. Wilk, and M. Koch, "Highly accurate optical material parameter determination with THz time-domain spectroscopy," Opt. Express **15**(7), 4335–4350 (2007).
25. L. Duvillaret, F. Garet, and J.-L. Coutaz, "A reliable method for extraction of material parameters in terahertz time-domain spectroscopy," IEEE J. Sel. Top. Quantum Electron. **2**(3), 739–746 (1996).
26. L. Duvillaret, F. Garet, and J.-L. Coutaz, "Highly precise determination of optical constants and sample thickness in terahertz time-domain spectroscopy," Appl. Opt. **38**(2), 409–415 (1999).
27. J. C. Lagarias, J. A. Reeds, M. H. Wright, and P. E. Wright, "Convergence properties of the Nelder-Mead simplex method in low dimensions," SIAM J. Optim. **9**(1), 112–147 (1998).
28. M. Tinkham, "Energy gap interpretation of experiments on infrared transmission through superconducting films," Phys. Rev. **104**(3), 845–846 (1956).
29. J. Dai, J. Zhang, W. Zhang, and D. Grischkowsky, "Terahertz time-domain spectroscopy characterization of the far-infrared absorption and index of refraction of high-resistivity, float-zone silicon," J. Opt. Soc. Am. B **21**(7), 1379 (2004).
30. M. Dressel and G. Grüner, *Electrodynamics of Solids: Optical Properties of Electrons in Matter* (Cambridge University Press, 2002).
31. I. Hamberg and C. G. Granqvist, "Dielectric function of "undoped" In_2O_3," Thin Solid Films **105**(2), L83–L86 (1983).
32. R. J. Collins and D. A. Kleinman, "Infrared reflectivity of zinc oxide," J. Phys. Chem. **11**, 190–194 (1959).

1. Introduction

Transparent conducting oxides (TCO) have attracted significant attention as alternative plasmonic materials to conventional metals [1–3]. Many studies focus on impurity doped zinc oxides [4–7], like aluminum- or gallium doped zinc oxide (AZO and GZO), and tin-doped indium oxide (ITO) [8] due to their low loss and metallic behavior in the near infrared. With the emerging of terahertz time domain spectroscopy (THz-TDS), the frequency resolved conductive properties of a range of conductors, including thin gold films [9], highly doped silicon [10,11] and ITO [8] have been investigated between 0.2 and 2.7 THz. However, no

#228530 - $15.00 USD Received 25 Nov 2014; revised 29 Jan 2015; accepted 3 Feb 2015; published 12 Feb 2015

broadband characterization of the complex conductivities of these TCO films has been performed in the THz range thus far. Compared to conventional metals, TCO films have much lower free-carrier concentration but still high enough to retain metallic functionality in the optical (near-infrared) and longer wavelength ranges where they can find plasmonic applications. Therefore it is important to experimentally characterize these TCOs over all these spectral ranges, and especially in the broad terahertz frequency range where there are no reports available thus far.

Recently, due to the development of two-color femtosecond air plasma THz-TDS [12–14], it has become possible to extend THz-TDS measurements on chalcogenide glasses [15] and water [16] up to 18 THz. Here we report the complex conductivities of ITO, AZO and GZO up to >18 THz covering the important crossover point where the scattering rate equals the frequency, $\omega\tau = 1$, thus allowing precise determination of the scattering time τ. We find that the ITO conductivities are well described by the simple Drude model, while the conductivity of GZO and AZO must be described by a Lorentz oscillator model in addition to the Drude response in order to take the phonon response of zinc oxide (ZnO) into account [5]. The experiments were performed with broadband laser induced plasma THz-TDS, supplemented by traditional photoconductive antenna (PCA)-based THz-TDS [17]. The complex conductivities were extracted through a customized thin film conductivity extraction algorithm. By additionally performing a Fourier transform infrared spectroscopy (FTIR) and ellipsometric measurements, we get the transmittance of the TCOs over an exceedingly broad frequency range from 0.5 THz to 1000 THz.

2. Samples and measurement techniques

To investigate the optical properties of TCOs, we prepared 6 wt% GZO, 2 wt% AZO and 10 wt% ITO samples of various thicknesses (from 110 nm to 260 nm) by using pulsed laser deposition (PLD) similar to the approach used in [5]. As shown in the inset of Fig. 1(a), the thin conducting films are deposited on top of a 525 μm thick high resistivity silicon (HR Si) substrate with a size of 1.5 cm by 1.5 cm, where the bare HR Si section of the sample is used as a reference. We used photoconductive antenna (0.5-2 THz) and broadband air plasma (1.5-18 THz) based THz-TDS and standard FTIR to characterize the TCO films in a broadband spectral range.

2.1 Traditional photoconductive antenna

A fiber coupled, commercial PCA-based THz-TDS system (Picometrix T-Ray 4000) was used to cover the frequency range from 0.5 to 2 THz [17]. The system has a fast scan time window of 320 ps with time resolution of 78 fs. The directly transmitted pulses of the time domain terahertz waveform measured in our experiment are shown in Fig. 1(a). The pulse is well isolated from the Fabry-Perot (FP) reflections inside the substrate, which is selected by using a window function before the numerical extraction of the conductivity of thin film. Due to the small thickness of the TCO layer, the overlapping Fabry-Perot (FP) reflections inside the TCOs need to be included in the conductivity extraction process, as will be briefly discussed below.

2.2 Broadband air plasma

Ultrabroadband terahertz pulses are generated by focusing 35 fs, 600 μJ, 800 nm wavelength pulses and their second harmonic at 400 nm to induce an air plasma which emits a broadband THz transient in a conical pattern as a result of the transient photocurrent in the plasma [18,19]. The temporal shape of the transmitted THz transient is detected by the air biased coherent detection (ABCD) method [20]. A typical terahertz pulse from this setup is shown in Fig. 1(b), with the corresponding amplitude spectrum plotted in Fig. 1(c). The terahertz pulse has time duration less than100 fs and the spectral coverage is up to 30 THz. A high-

#228530 - $15.00 USD Received 25 Nov 2014; revised 29 Jan 2015; accepted 3 Feb 2015; published 12 Feb 2015

resistivity (HR) Si beam splitter which induces a dip at 18.5 THz due to a weak phonon overtone [21,22] is inserted into the THz generation beam path to block 800/400 nm light.

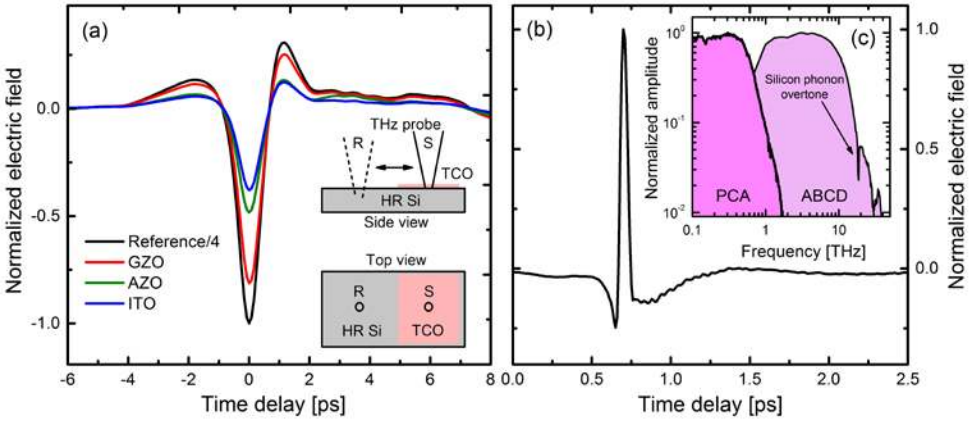

Fig. 1. (a) Time traces of terahertz pulses generated by photoconductive antenna transmitted through 525 µm thick HR Si (black line) scaled down by a factor of 4 for comparision, 525 µm thick HR Si with 215 nm thick GZO (red line), 260 nm thick AZO (green line) and 210 nm thick ITO (blue line). Inset: sketch of the sample and illumination geometry. (b) Time trace of terahertz pulse generated by air plasma. Inset of (b): (c) the amplitude spectra of the PCA and air plasma THz pulses.

3. Extraction of the complex conductivity of the film

Accurate extraction of optical parameters with methods extending beyond the simple analysis of a single-pass transmission of the THz field through the sample is well documented in the literature [23–26]. We use a method based on the same principles, adapted to take into account that the sample of interest in our case is a thin, conductive film placed on a dielectric substrate. The film is characterized by its complex-valued conductivity $\tilde{\sigma}(\omega) = \sigma'(\omega) + i\sigma''(\omega)$.

Starting with the experimental time traces of the THz signal transmitted through the thin film on substrate and the substrate alone, (labeled $E_{film}(t)$ and $E_{sub}(t)$ respectively), we Fourier transform these traces ($E_{film}(t) \to \tilde{E}_{film}(\omega), E_{sub}(t) \to \tilde{E}_{sub}(\omega)$) and calculate the experimental transfer function $\tilde{T}_{exp}(\omega) = \tilde{E}_{film}(\omega) / \tilde{E}_{sub}(\omega) \equiv A_{exp}(\omega)\exp[i\theta_{exp}(\omega)]$. This transfer function is then compared to the theoretical transfer function $\tilde{T}_{calc}(\omega) \equiv A_{calc}(\omega)\exp[i\theta_{calc}(\omega)]$ which describes the transmission through the air-oxide-Si-air interface system relative to the transmission through air-Si-air interface system. This theoretical transfer function $\tilde{T}_{calc}(\omega)$ is described by the conductivity of the thin film without any a priori assumptions about the actual spectral shape of $\tilde{\sigma}(\omega)$, using the standard Fresnel interface equations and wave propagation terms inside bulk materials and summing up the infinite number of THz wave bounces inside the oxide film. The algorithm to extract the best estimate of the conductivity of the thin film is an iterative process which minimizes the error function [25]

$$\Delta(\omega) = \left(A_{calc}(\omega) - A_{exp}(\omega)\right)^2 + \left|\theta_{calc}(\omega) - \theta_{exp}(\omega)\right| \quad (1)$$

#228530 - $15.00 USD Received 25 Nov 2014; revised 29 Jan 2015; accepted 3 Feb 2015; published 12 Feb 2015

by simultaneously finding optimal $\sigma'(\omega)$ and $\sigma''(\omega)$ by using the standard Nelder-Mead Simplex Method [27]. As the initial guess for $\sigma'(\omega)$ and $\sigma''(\omega)$ we use values obtained from the Tinkham thin film equations which are based on a single pass of the electromagnetic field through the film [28], as commonly applied to calculate the complex conductivity in the low frequency region.

$$\sigma'_{init}(\omega) = \frac{n_{sub}+1}{Z_0 d}\left[\frac{\cos(\theta_{exp}(\omega))}{A_{exp}(\omega)} - 1\right] \tag{2}$$

$$\sigma''_{init}(\omega) = -\frac{n_{sub}+1}{Z_0 d}\cdot\frac{\sin(\theta_{exp}(\omega))}{A_{exp}(\omega)}, \tag{3}$$

where $n_{sub} = 3.4177$ is the refractive index of the high resistivity silicon substrate [29], d is the film thickness and Z_0 is the free space impedance. These values obtained from the thin film Eqs. (2) and (3) are burdened with a systematic error, because their validity criterion $n_{film} d\omega / c \ll 1$ does not necessarily hold for high-index films at high frequencies. As a result, we find differences between the minimization algorithm result and the Tinkham thin film equations as high as 30% at frequencies higher than 10 THz for the investigated films, highlighting the strict requirements on the methodology for precise determination of the optical conductivity of thin films especially at high frequencies.

4. Complex refractive index

The complex index of refraction can be directly calculated from the extracted complex conductivity [30]. Figure 2 shows the index of refraction ($\tilde{n} = n + i\kappa, \alpha = 2\kappa\omega / c$) from air plasma THz-TDS measurements for ITO, AZO and GZO. The TCOs have very high refractive index up to 55 (110 nm thick ITO at 1.5 THz). Both AZO and GZO show a lower absorption and are less conductive (see Fig. 3) than ITO. For the whole frequency range, the real part of the refractive index of ITO is higher than that of AZO and GZO, with no discernible difference between GZO and AZO. The periodic structure near 2 THz for both AZO and GZO is due to the low signal to noise ratio in this region.

#228530 - $15.00 USD Received 25 Nov 2014; revised 29 Jan 2015; accepted 3 Feb 2015; published 12 Feb 2015

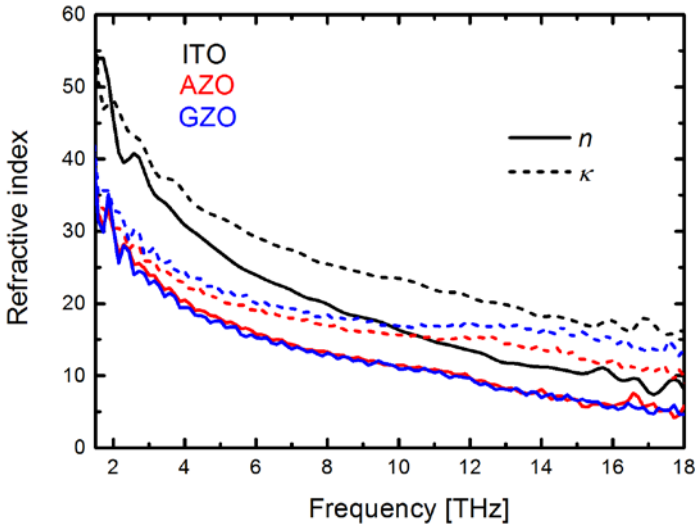

Fig. 2. Optical constants of TCOs: 110 nm thick ITO (black), 140 nm thick AZO (red) and 122 nm thick GZO (blue), with real (solid lines) and imaginary (dashed lines) parts of the complex index of refraction.

5. Drude and Drude-Lorentz fit

In order to account for the combined conductivity and phonon response of the materials, we use the Drude model and Drude-Lorentz oscillator model to parametrize the extracted complex conductivity. The Drude model is used to describe free carrier response in bulk solids, and the Lorentz oscillator describes bound charges (in this case the phonon response) with a certain resonance frequency. In both cases, the fitting parameters were obtained by simultaneously fitting the model to the measured real and imaginary conductivity data. For the Drude model, the real and imaginary parts of the conductivity are described by

$$\sigma'(\omega) = \frac{\sigma_{dc}}{1+(\omega\tau)^2}, \tag{4}$$

$$\sigma''(\omega) = \frac{\sigma_{dc}\omega\tau}{1+(\omega\tau)^2}. \tag{5}$$

For the Drude-Lorentz model, the real and imaginary parts of the conductivity are described by

$$\sigma'(\omega) = \frac{\sigma_{dc}}{1+(\omega\tau)^2} + \frac{\varepsilon_0\omega_{pl}^2\omega^2\gamma}{(\omega_0^2-\omega^2)^2+(\omega\gamma)^2}, \tag{6}$$

$$\sigma''(\omega) = \frac{\sigma_{dc}\omega\tau}{1+(\omega\tau)^2} - \frac{\varepsilon_0\omega_{pl}^2\omega(\omega_0^2-\omega^2)}{(\omega_0^2-\omega^2)^2+(\omega\gamma)^2}, \tag{7}$$

where σ_{dc}, τ is the Drude dc conductivity and scattering time, respectively, and $\omega_{pl}, \omega_0, \gamma$ is the Lorentz plasma frequency, resonance frequency and damping rate, respectively. The Drude plasma frequency is calculated as $\omega_{pd} = \sqrt{\sigma_{dc}/(\varepsilon_0\tau)}$.

#228530 - $15.00 USD Received 25 Nov 2014; revised 29 Jan 2015; accepted 3 Feb 2015; published 12 Feb 2015

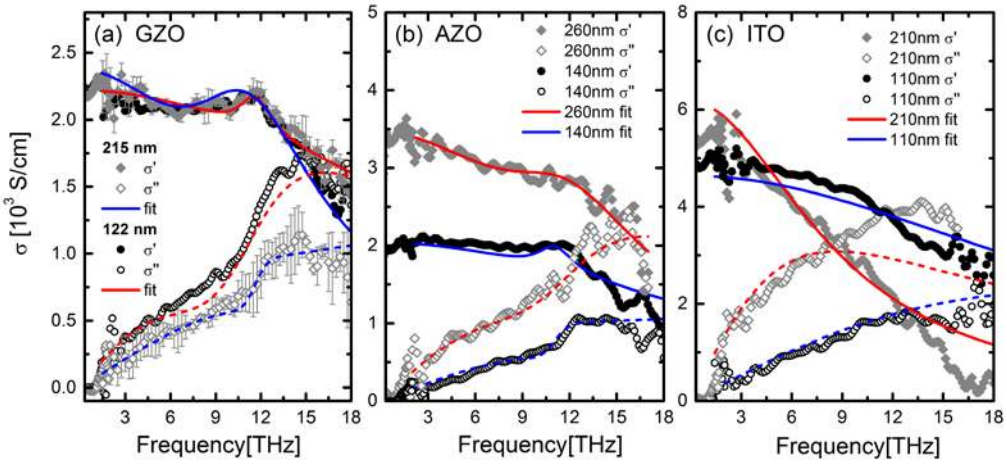

Fig. 3. The extracted real (filled symbols) and imaginary (open symbols) parts of the complex conductivity of the TCOs. Drude-Lorentz fits (red and blue curves) up to 18 THz for (a) GZO and (b) AZO. (c) Drude fits to 18 THz for ITO. The error bars for 215 nm thick GZO is the standard deviation calculated from 3 measurements, which is also representative for AZO and ITO measurements. The data between 0.5 and 2 THz were obtained with PCA measurements.

For both GZO and AZO we find good Drude fits if the frequency range is confined to below 8 THz. However, a good representation of the full range up to 18 THz can only be obtained with the combined Drude-Lorentz fits (as shown in Fig. 3(a) and 3(b)). The real part of the conductivity of 215 nm and 122 nm thick GZO overlap well with each other, while the difference between the imaginary parts is significant for the full spectral range up to 18 THz, as seen in Fig. 3(a). From the fit parameters shown in Tables 1 and 2, we see that the 122 nm thick GZO has a longer scattering time than the 215 nm thick sample. For AZO, the 260 nm thick sample is much more conductive and has a longer scattering time, than the thinner sample (140 nm). We believe that this difference in conductivity for different AZO samples could be caused by the interface with the substrate, which can have many carrier trap states which reduce the net carrier concentration [5]. We obtain a good Drude fit for 110 nm thick ITO up to 11 THz and reasonable Drude fit up to 18 THz (as shown in Fig. 3(c)), while the Drude model only fits well up to 8 THz for the 210 nm thick ITO. Measurements on thin films produced by electron beam deposition have shown that undoped ITO has three closely spaced phonon modes in the range 8.7-13.7 THz [31]. While we do not resolve these three individual modes in our measurements, the observed deviation from the Drude response is very likely due to these phonon modes.

Figure 3(a, b, c) shows that the optical conductivity of all the thin film materials is thickness dependent, which based on the current results is most likely due to minor variations in the deposition conditions as well as the varying ratio of bulk to interface contributions such as surface state electrons, to the optical conductivity.

The plots between 0.5 THz and 2 THz in Fig. 3(a, b, c) are extracted from PCA measurements, and overlap very well with the air plasma measurements, thus confirming the absolute values of the reported data. The large variation of the optical properties with film thickness can be an indication of the importance of the deposition conditions. For instance, Chen *et al.* [8] used THz-TDS and Hall measurements to characterize ITO films of similar thickness, reporting dc conductivities in the range 1500-2200 $\Omega^{-1}cm^{-1}$, significantly lower than our measurements, and a scattering time of 5.8-6.9 fs, comparable to our measurements on the 110-nm film, but significantly lower than our measurement (16.7 fs) on the 210-nm film.

#228530 - $15.00 USD Received 25 Nov 2014; revised 29 Jan 2015; accepted 3 Feb 2015; published 12 Feb 2015

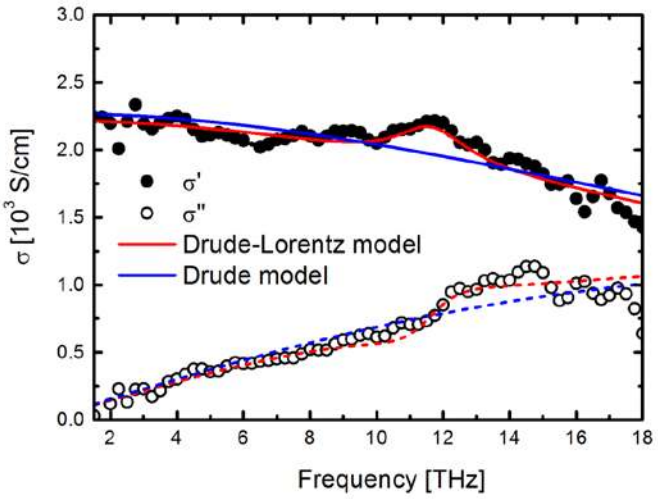

Fig. 4. Comparison between Drude fit (blue lines) and Drude-Lorentz fit (green lines) for the extracted complex conductivity of 215 nm thick GZO. The real and imaginary parts are plotted in dots and open circles, respectively.

A comparison between the lower-frequency Drude fits with the full Drude-Lorentz fits up to 18 THz for GZO highlights the importance of including the high-frequency phonon response in order to extract reliable physical parameters from the experimental data, as shown in Fig. 4. Due to the presence of the ZnO phonon resonance at 12 THz [32], an evident change from a pure Drude conductivity response is observed. The phonon resonance is responsible for the breakdown of the Drude fit when considering the full spectral range (1.5 – 18.0 THz). A Drude fit without a Lorentz term seemingly fits well to the measured complex conductivity up to 8 THz, below the ZnO resonance. However, due to the low-frequency tail of the phonon resonance, the Drude scattering time (τ_1) is lower from the Drude fits (up to 8 THz) than from the Drude-Lorentz fits (up to 18 THz), see Table 1 and Table 2.

Table 1. Fit parameters extracted from Drude fits to 8 THz

Material	d	τ	$\omega_{pd}/2\pi$	σ_{dc}
	[nm]	[fs]	[THz]	[(Ω·cm)$^{-1}$]
ITO	210	16.7 ± 0.4	316	5815 ± 72
ITO	110	5.4 ± 0.1	506	4842 ± 20
GZO	215	5.0 ± 0.2	355	2200 ± 16
GZO	122	7.5 ± 0.1	291	2222 ± 12
AZO	260	7.7 ± 0.2	352	3340 ± 24
AZO	140	4.8 ± 0.1	352	2080 ± 7

Table 2. Fit parameters extracted from Drude-Lorentz fits to 18 THz in Fig. 3

Material	d	τ	$\omega_{pd}/2\pi$	σ_{dc}	γ	$\omega_0/2\pi$	$\omega_{pl}/2\pi$
	[nm]	[fs]	[THz]	[(Ω·cm)$^{-1}$]	[THz]	[THz]	[THz]
ITO[a]	210	-	-	-	-	-	-
ITO	110	6.2 ± 0.1	462	4637 ± 31	-	-	-
GZO	215	5.5 ± 0.1	340	2219 ± 14	16.4 ± 3.2	11.6 ± 0.1	35 ± 3
GZO	122	14.4 ± 1.5	217	2376 ± 22	64.1 ± 4.1	11.7 ± 0.1	137 ± 12
AZO	260	11.7 ± 1.3	291	3456 ± 25	65.8 ± 11.3	12.5 ± 0.1	130 ± 23
AZO	140	6.7 ± 0.1	295	2041 ± 16	17.5 ± 3.2	11.1 ± 0.1	39 ± 3

[a]The complex conductivity of ITO is fitted by pure Drude model. Because of the poor fit due to the complex phonon band in the 9-14 THz range, the fit parameters for the 210-nm ITO film to 18 THz are not given.

#228530 - $15.00 USD Received 25 Nov 2014; revised 29 Jan 2015; accepted 3 Feb 2015; published 12 Feb 2015

6. FTIR and ellipsometry measurements

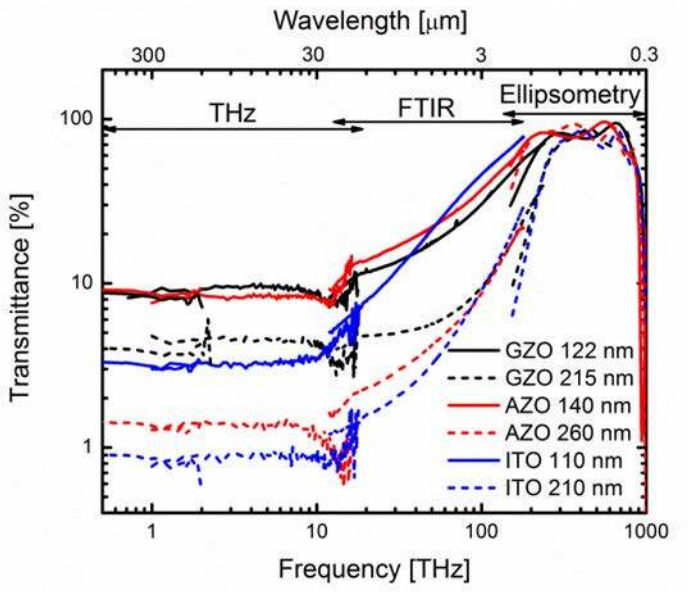

Fig. 5. Transmittance of GZO, AZO and ITO from 0.5 THz to 1000 THz measured with THz-TDS, FTIR spectroscopy and ellipsometry.

We have also performed FTIR measurements closing the gap between terahertz (0.5-18 THz) and ellipsometry (200-1000 THz) measurements. The consolidated transmittance curves measured by THz-TDS, FTIR and extracted from ellipsometry measurements are displayed in Fig. 5. A simple model of a conductive oxide slab sandwiched between two air slabs was used to calculate the transmittance from the complex permittivity obtained from ellipsometry measurements. A slight deviation is observed at the overlap region (150-200 THz) which may be caused by the fact that we have not taken into account that the conductive oxide slab is surrounded by silicon from one side and not air for FTIR measurements. The slight deviation could also be partly due to the ellipsometry measurements for AZO being performed on different samples with the thicknesses 149 nm and 264 nm, and for ITO, measurement was performed with the same 234 nm thick sample. Nevertheless, there is a reasonable continuity from THz-TDS measurements to ellipsometry measurements.

7. Conclusion

In conclusion, we have retrieved broadband optical conductivities in the 0.5-18 THz (17-600 cm^{-1}, 2-74 meV) range of transparent conducting oxides, GZO, AZO and ITO, with different layer thicknesses using PCA and ultrabroadband air plasma THz spectroscopy. The conductivities were extracted with an iterative thin film extraction algorithm and analyzed by fitting with the Drude model for ITO and Drude-Lorentz oscillator model for GZO and AZO. The additional resonance term in GZO and AZO originates from the ZnO phonon at 12 THz. In ITO, the optical properties above 9 THz are influenced by a strong, broad band of several phonon modes. For GZO and AZO, we find the electron scattering time obtained from the Drude-Lorentz model is more reliable than the Drude model due to the ZnO phonon resonance, highlighting the requirement of an ultrabroadband measurement technique in order to fully understand conductivity dynamics in metal oxides. The conductivity of AZO is found to be more thickness dependent than GZO and ITO, indicating high importance of surface states and growth conditions for electron dynamics in AZO, and our results suggest that further investigation of the detailed dependence on the fabrication conditions will be valuable.

#228530 - $15.00 USD Received 25 Nov 2014; revised 29 Jan 2015; accepted 3 Feb 2015; published 12 Feb 2015

We have also shown the transmittance of these TCOs from 0.5 THz to 1000 THz by performing FTIR measurements bridging the gap between THz-TDS and ellipsometry data. The reported results will contribute to a better exploitation of these metal oxide systems in plasmonic applications where tailored conductivity properties of the metal are needed.

Acknowledgments

We acknowledge partial financial support from the Danish Council for Independent Research through Projects THz-COW and HI-TERA (FTP) and THz-BREW (FNU). The Purdue group acknowledges support from the Office of Naval Research (ONR), MURI grant N00014-10-1-0942.